Robust Interference Mitigation techniques for Direct Position Estimation

Haoqing Li
Northeastern University, Boston, MA 02115, USA

Shuo Tang
Northeastern University, Boston, MA 02115, USA

Peng Wu
Northeastern University, Boston, MA 02115, USA

Pau Closas, Senior Member, IEEE
Northeastern University, Boston, MA 02115, USA

***Abstract*— Global Navigation Satellite System (GNSS) is pervasive in navigation and positioning applications, where precise position and time referencing estimations are required. Conventional methods for GNSS positioning involves a two-step process, where intermediate measurements such as Doppler shift and time delay of received GNSS signals are computed and then used to solve for the receiver's position. Alternatively, Direct Position Estimation (DPE) was proposed to infer the position directly from the sampled signal without intermediate variables, yielding to superior levels of sensitivity and operation under challenging environments. However, the positioning resilience of DPE method is still under the threat of various interferences. Robust Interference Mitigation (RIM) processing has been studied and proved to be efficient against various interference in conventional two-step positioning (2SP) methods, and therefore worthy to be explored regarding its potential to enhance DPE. This article extends DPE methodology by incorporating RIM strategies that address the increasing need to protect GNSS receivers against intentional or unintentional interferences, such as jamming signals, which can deny GNSS-based positioning. RIM, which leverages robust statistics, was shown to provide competitive results in two-step approaches and is here employed in a high-sensitivity DPE framework with successful results. The article also provides a quantification of the loss of efficiency of using RIM when no interference is present and validates the proposed methodology on relevant interference cases, while the approach can be used to mitigate other common interference signals.**

***Index Terms*— GNSS, Direct Positioning, Robust Interference Mitigation, Anti-Jamming, Robust statistics.**

This work has been partially supported by the National Science Foundation under Awards ECCS-1845833 and CCF-2326559.

Authors are with the Department of Electrical and Computer Engineering at Northeastern University, 360 Huntington Avenue, Boston, MA 02115 (USA). e-mail: {li.haoq, tang.shu, wu.p, closas}@northeastern.edu

I. Introduction

The conventional approach to process GNSS signals is a 2SP process, where the so-called Cross Ambiguity Function (CAF) is computed and maximized as a function of time delay and Doppler shift of each in-view satellite [1]–[3]. The GNSS solution including position and velocity of a GNSS receiver is then calculated based on the time delay and Doppler shift from the first step. Despite of the generality and efficiency of the 2SP approach, the fact that intermediate measurements (Doppler shift and time delay) are used would degrade the performance compared with the case when position is directly estimated in one step, which is the DPE approach. This is proved in [4], [5] showing the performance of DPE approach can never be worse than the 2SP approach. One of the main benefits of DPE processing is that receivers can increase their senstivity, thus being able to operate at lower signal-to-noise ratios compared to their 2SP versions [6].

DPE for GNSS was first proposed in [7]. This approach is based on the fact that time delays and Doppler shifts of all satellites are intimately related to one another through the GNSS solution of receiver. Considering the CAF as a function of Position Velocity and Time (PVT) of GNSS receiver, the PVT results can be acquired in just one step by maximizing the CAF. Compared with conventional 2SP approach, DPE approach has following advantages [6]: i) no intermediate measurements: as discussed above, 2SP approach needs to estimate Doppler shift and time delay parameters for GNSS solution, which brings potential correlation among channels and propagation effects. Those errors would cause further distortions in GNSS solution through non-linearity; ii) lower dimension size: since 2SP approach needs to estimate Doppler shift and time delay of every available channel, the dimension size can simply increase to a larger value especially in a multi-constellation receiver, while DPE approach only need to estimate PVT solution; iii) simpler syncronization problem: The prior information from the tracking loops in 2SP approach is generally applied as an involved task [8] and would need extensive test-field campaigns to generate relevant data [9], and the algorithm needs to clarify among difference synchronization evolution models based on the dynamics of receiver. This is much more difficult compared with the case when the parameter of interest is the user's position itself, with each parameter has their own physical meaning to aid the inclusion of side information; iv) robustness, DPE approach is more robust than 2SP approach against interferences, given the estimation of position is jointly performed taking into account measurements from all in–view satellites [7], [10].

However, regardless of the robustness of DPE compared with 2SP approach, the interferences can still cause a degradation to its performance. Such interferences, such as intentional jammers or unintentional interferences [11], become challenging threats in the GNSS processing chain. Despite of the fact that jammers are illegal devices in

most (not all) countries, they are very easy to built and cheap to buy, those devices can cause a large-area disruption to GNSS-based services (in kilometers level). In addition, unintentional interferences can also be a problem in GNSS positioning. For example, the Distance Measuring Equipment (DME) signal, which is essential in aircraft navigation, or other technologies are known to interfere GNSS signals [12]–[14]. Therefore, the research of interference mitigation techniques have been triggered recently.

In terms of the 2SP approach, a classical jamming signal mitigation method is Interference Cancellation (IC), in which the detection, estimation and reconstruction of the interference waveform is done. For instance, pulse blanking and (adaptive) notch filtering [15], [16] are the two typical and popular IC methods. However, the drawback of this approach cannot be neglected, where detection and estimation are two possible causes of failure during processing, and that there is a need to make assumptions on the jamming signal waveform [17]. To overcome those drawbacks, a robust statistics based approach was investigated, where interferences are regarded as outliers. It is referred to as RIM approach, in which the estimation of the interference waveform and its detection can be avoided. The concept was first implemented in [18], where the RIM approach acts as a filter to mitigate pulsed interference as outliers in received signal. In [18], the myriad Zero Memory Non-Linearity (ZMNL) was derived by substituting the classical Gaussian assumption with Cauchy assumption on the jammed input signal, while the complex signum ZMNL, is derived under a Laplacian model in [19]. Both works apply their ZMNLs in time domain, under a more relaxed assumption of heavy-tailed Probability Density Function (PDF) to the noise statistics, modelling large outliers in the sampled signal. Then, [20]–[22] explored the use of Huber's ZMNL in transformed domain instead of the time one. Furthermore, [23] studied Huber's ZMNL in multiple domains, both time and transformed, which was referred to as Dual-Domain RIM. Recently, [24] has discussed the jointly use of RIM approach and other typical interference mitigation techniques in multi-layer multi-constellation GNSS processing. In this paper, we study the potential of RIM approach in DPE processing, considering Huber's ZMNL to single- and dual-domains, exploring the performances of them in the presence and absence of different kinds of jamming signals. Specifically, intentional Continuous Wave (CW) jamming signal and DME interference signal. Notice that RIM, which DPE-RIM is based on, is effective against interference signals that can be considered to be outliers in time (e.g. pulsed interferences), frequency (e.g. CW), in arbitrary domains (e.g. wavelet transform), or in multiple domains (e.g. the case of the DME signal) [23]. As a consequence, RIM (and therefore DPE-RIM) could be applicable to wideband interferences when these appear as pulsed in time domain, otherwise this methodology is not applicable and other solutions such as the use of antenna arrays may be considered [25].

In summary, the main novel contributions of this article with respect to previously published works are:

- A robust DPE receiver solution that mitigates interferences through the incorporation of RIM methodology. This results in a novel GNSS receiver framework that features high-sensitivity and interference rejection.
- Analysis of the Loss of Efficiency (LoE) of such approach in terms of the Cramér–Rao Bound (CRB) degradation under a direct-positioning framework.
- Performance analysis of a specific RIM method (based on Huber's non-linearity) under direct-positioning framework against CW and DME interferences, validating the theoretical results.

The remainder of the paper is organized as follows: Section II describes the signal model for both GNSS and interference signals, as well as recalls the basics of DPE processing. Section III contains the main contribution, showing the application of RIM to DPE. Section IV provides a discussion and the derivation of LoE of RIM under DPE, which corresponds to the degradation of using RIM when there is no interference present. Section V details the simulation experiments and corresponding analysis. Finally, the paper concludes with final remarks in Section VI.

II. Signal models and direct-positioning background

This section provides a discussion on the signal models for GNSS signals and interference signals that are used later in the article. Particularly, we formulate the signal model for a generic intentional jammer and the DME signal, the latter being a type of unintentional interference that is explored in the simulations result. This section also provides a review of DPE signal processing, which will be augmented with the RIM approach in Section III.

A. Signal Model

As described in [6], [26], the complex baseband equivalent of the received signal at an antenna can be modeled as the summation of several scaled, structure-known signals with time delay and Doppler shift as shown below:

$$x(t) = \sum_{i=1}^{M} \alpha_i c_i(t-\tau_i) \mathrm{e}^{j(2\pi f_{d,i} t + \phi_i)} + \eta(t) + i(t) \quad (1)$$

where M is the number of satellites that are visible to the receiver, the index $i \in \{1, \cdots M\}$ denotes each satellite, α_i is the complex amplitude containing phase information, $c_i(t)$ is the complex navigation signal spread by the corresponding Pseudo-Random Noise (PRN) code, τ_i is the time delay from the satellite to the receiver, $f_{d,i}$ is the Doppler shift, $\eta(t)$ denotes Additive White Gaussian Noise (AWGN) signal with double sided spectral density $N_0/2$, and ϕ_i denotes the phase shift introduced by the communication channel, which is regarded as an unknown

parameters alongside τ_i and $f_{d,i}$. In the absence of interference $\eta(t)$ is the dominating random term and the reason for assuming that $x(t)$ follows a Gaussian distribution. When an interference is present, $i(t)$, the noise component $\eta(t) + i(t)$ would incorporate both contributions. In this paper, $i(t)$ is modeled as a generic signal, and can be, for instance, a CW jamming signal or a DME interference signal as will be described later in this section. The covariance of the noise is defined as

$$\mathbb{E}\{\eta(t)\eta(t)^H\} = \sigma_n^2 \,. \tag{2}$$

It is noted that the noise signal is circularly-symmetric complex Gaussian such that the real and imaginary parts have the same variance $\sigma_n^2/2$. After sampling at a suitable rate $f_s = \frac{1}{T_s}$ that satisfies the Nyquist criterion, the resulting complex discrete-time sequence is:

$$x[n] = \sum_{i=1}^{M} \alpha_i c_i(nT_s - \tau_i) \mathrm{e}^{j(2\pi f_{d,i} n T_s + \phi_i)} + \eta[n] + i[n] \tag{3}$$

B. Interference signal

The baseband interference signal, $i[n]$, can assume different forms depending on the type of source generating it [27], [28]. A wide class of interference signals can be modeled as

$$i[n] = \alpha_I \mathrm{e}^{j2\pi f_I[n] n T_s + j\phi_I[n]} \,, \tag{4}$$

that is, signals with a constant amplitude, α_I, and a time-varying frequency/phase, $f_I[n]$ and $\phi_I[n]$ respectively. For instance, CW interferences can be modeled as (4) with some constant parameters $f_I[n] = f_{CW} = \text{const}$ and $\phi_I[n] = \phi_{CW} = \text{const}$. When the interference amplitude is assumed constant, the signal model (4) is not able to capture pulsed signals such as DME components. Due to its relevance in the context of GNSS, DME signals are specifically discussed in the next section.

C. Distance Measurement Equipment signal model

DME is used to measure the distance between aircraft and ground station by measuring the propagation delay between a DME interrogator equipment onboard the aircraft and a transponder at the ground station. It operates in four modes: X, Y, W and Z, between 960 MHz and 1215 MHz in an Aeronautical Radionavigation Services (ARNS) band [12]. In particular, the X-mode replies in $1151 - 1213$ MHz, which thus overlaps with the GNSS $E5$ and $L5$ bands. For this reason, GNSS signal reception in the $E5$ and $L5$ band can be degraded by DME signals. Therefore, DMEs replying in X-mode can interfere with GNSS signal reception and should be mitigated.

DME signals are composed of pulse pairs and Fig. 1 shows one pair of DME signal in time domain. As shown in the figure, considering its short time duration and high peak power, the DME signal can be regarded as an outlier in the time domain. Moreover, when considering its Power Spectral Density (PSD) in [12], DME signals can also be considered as an outlier in the frequency domain due to its high power concentrated in a narrow band. More details of the parameters and modeling of DME signals can be found in [12], [29].

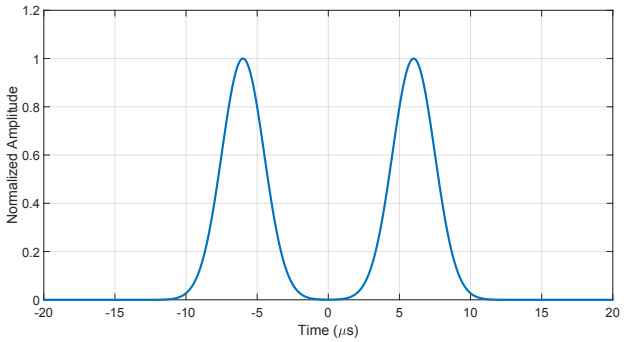

Fig. 1. Example of DME signal waveform with normalized amplitude.

D. Direct Position Estimation

The signal model in (1), typically considered in most receiver designs [3], assumed that delay and Doppler are constant within an observation window (the integration interval). However, in practice, these quantities evolve over time as a consequence of their physical interpretation [30]. We review this in this section, while we notice that time delay and Doppler shifts can be parameterized by the position of the receiver, as well as the time-varying positions and velocities of the satellites. Particularly, the time delay – or the signal propagation time –, is related to the distance between the satellite and the receiver. Consequently, the pseudorange observable $\rho_i = c\tau_i$ is modeled as

$$\rho_i = \varrho_i(\boldsymbol{p}) + c(\delta t - \delta t_i) + \epsilon_i, \tag{5}$$

$\varrho_i(\boldsymbol{p})$	$\|\|\boldsymbol{p} - \boldsymbol{p}_i\|\|$ between the i-th satellite, located at position $\boldsymbol{p}_i = (x_i, y_i, z_i)^\top$, and the receiver, whose position $\boldsymbol{p} = (x, y, z)^\top$ is unknown;
c	is the speed of light in m/s;
δt	the unknown receiver clock bias with respect to GNSS time;
δt_i	the i-th satellite clock bias with respect to GNSS time given by the ephemeries; and
ϵ_i	a random term including ephemeris errors, atmospheric-induced delays, relativistic effects, and other unmodeled errors.

The Doppler shift is the difference between the observed carrier frequency and its nominal value at transmission. The Doppler effect is caused by the relative motion between the receiver and the corresponding satellite. The Doppler shift can be modeled as

$$f_{d,i} = -(\boldsymbol{v}_i - \boldsymbol{v})^\top \boldsymbol{u}_i (1 + \dot{\delta t}) \frac{f_c}{c}, \tag{6}$$

where $\boldsymbol{v}_i = (v_{x,i}, v_{y,i}, v_{z,i})^\top$ is the velocity vector of the i-th satellite, $\boldsymbol{v} = (v_x, v_y, v_z)^\top$ is the velocity of

the receiver, $\dot{\delta t}$ is the clock drift of the receiver, and $\boldsymbol{u}_i$ denotes the unit vector from the receiver pointing to the i-th satellite as $\boldsymbol{u}_i = \frac{\boldsymbol{p}_i - \boldsymbol{p}}{||\boldsymbol{p}_i - \boldsymbol{p}||}$, where $||\cdot||$ denotes the ℓ_2-norm of a vector and f_c denotes the carrier frequency of the transmitted GNSS signal.

As shown in (5) and (6), the delay τ_i and Doppler shift $f_{d,i}$ of the i-th satellite are functions of the position $\boldsymbol{p}$ and velocity $\boldsymbol{v}$ of the receiver. More generally, if we gather all dynamics-related unknown parameters into a vector $\boldsymbol{\kappa}$ (for instance, $\boldsymbol{\kappa} = \boldsymbol{p}$ or $\boldsymbol{\kappa}^\top = (\boldsymbol{p}^\top, \boldsymbol{v}^\top)$ [6]), the signal model in (1) can be parameterized by $\boldsymbol{\kappa}$

$$x(t) = \sum_{i=1}^{M} \alpha_i c_i(t - \tau_i(\boldsymbol{\kappa}))\mathrm{e}^{j(2\pi f_{d,i}(\boldsymbol{\kappa})t + \phi_i)} + \eta(t) + i(t) \tag{7}$$

After sampling at a $f_s = \frac{1}{T_s}$ that satisfies the Nyquist criterion, the resulting discrete-time complex signal is:

$$x[n] = \sum_{i=1}^{M} \alpha_i c_i(nT_s - \tau_i(\boldsymbol{\kappa}))\mathrm{e}^{j(2\pi f_{d,i}(\boldsymbol{\kappa})nT_s + \phi_i)} + \eta[n] + i[n] \tag{8}$$

DPE solves for the Maximum Likelihood (ML) estimation of $\boldsymbol{\kappa}$, given the model in (7). It can be seen [6] that maximizing such likelihood is equivalent to minimizing the cost function:

$$\Lambda(\boldsymbol{\kappa}) = \sum_{n=0}^{N-1} |x[n] - \sum_{i=1}^{M} \alpha_i c_i(nT_s - \tau_i(\boldsymbol{\kappa}))\mathrm{e}^{j(2\pi f_{d,i}(\boldsymbol{\kappa})nT_s + \phi_i)}|^2 \tag{9}$$

Following the derivation from [6], the estimate of $\boldsymbol{\kappa}$ is

$$\begin{aligned}\hat{\boldsymbol{\kappa}} &= \arg\max_{\boldsymbol{\kappa}} \left\{ \sum_{i=1}^{M} \left| \sum_{n=0}^{N-1} x[n] c_i(nT_s - \tau_i(\boldsymbol{\kappa}))\mathrm{e}^{-j(2\pi f_{d,i}(\boldsymbol{\kappa})nT_s)} \right|^2 \right\} \\ &= \arg\max_{\boldsymbol{\kappa}} \left\{ \sum_{i=1}^{M} |\mathcal{C}_i(\boldsymbol{\kappa})|^2 \right\}\end{aligned} \tag{10}$$

where $\mathcal{C}_i(\boldsymbol{\kappa})$ is the so-called CAF of the i-th satellite [3], defined as the correlation between the received samples and the local code, in this case parameterized by $\boldsymbol{\kappa}$. Notice that when carrier-phase is also parameterized by $\boldsymbol{\kappa}$ the resulting cost function would be different, in which case high-accuracy DPE would be enabled [31]. In this work we restrict to the typical DPE case where phase is considered unknown but independent of $\boldsymbol{\kappa}$ [6].

III. Robust Interference Mitigation and direct-positioning

This section discusses how the RIM approach can be incorporated in DPE approach. Particularly, its applicability in various domains is treated, namely: Transformed Domain (TD) and Dual Domain (DD). At a glance, RIM modifies the maximum likelihood cost function that typically results in (10) using a nonlinear function $\rho(\cdot)$, which produces estimates that are more robust to outliers. In this case, outliers are interference signals that are stronger than GNSS signals and sparse in one or several of the aforementioned domains [17]. In practice, RIM results in a variation of the CAF, which is referred to as a Robust CAF and denoted as $\mathcal{C}_{\rho,i}(\boldsymbol{\kappa})$ for the i-th satellite (cf. Appendix A). In the context of DPE, the resulting robust estimation of the parameters in $\boldsymbol{\kappa}$ is then

$$\hat{\boldsymbol{\kappa}} = \arg\max_{\boldsymbol{\kappa}} \left\{ \sum_{i=1}^{M} |\mathcal{C}_{\rho,i}(\boldsymbol{\kappa})|^2 \right\} \tag{11}$$

where the definition of depends on the time of RIM processing performed, as detailed in the following subsections. Notice that, in the case of 2SP, the RIM solution resembles (11) with the exception that there is no sum over satellites and that the CAF is parameterized by time delay and Doppler shift instead of $\boldsymbol{\kappa}$.

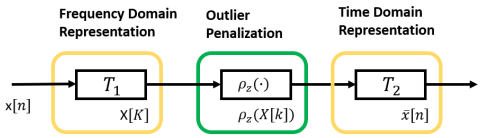

Fig. 2. Generic block diagram of RIM processing on signal samples.

A. RIM in TD

In RIM processing, the ZMNLs can be applied in general TDs, which is depicted in Fig. 2. A linear transform, $\mathbf{T}_1$, is used to project the interference component into a domain such that it occurs as a sparse representation, where only a limited number of samples are affected. Transform $\mathbf{T}_1$ produces the TD samples

$$X[k] = \mathbf{T}_1(x[n]). \tag{12}$$

The change of index, from n to k, is a notational convention adopted to indicate that the input samples, $x[n]$, have been brought to a different representation domain. Following $\mathbf{T}_1$, a ZMNL is used to reduce the impact of outliers in the TD. A generic ZMNL is denoted here as $\rho_z(\cdot)$ and produces the samples

$$X_{\rho_z}[k] = \rho_z(X[k]) \ . \tag{13}$$

Finally, a second linear transform, $\mathbf{T}_2$, is applied to the samples, $X_{\rho_z}[k]$ to obtain new, filtered time domain discrete-time signal. $\mathbf{T}_2$ inverts the effects of $\mathbf{T}_1$ and brings back the samples to the time domain. The output of $\mathbf{T}_2$ is denoted here as

$$\bar{x}[n] = \mathbf{T}_2(X_{\rho_z}[k]). \tag{14}$$

Therefore we can say that $\mathbf{T}_1$ and $\mathbf{T}_2$ are inverse operators, $\mathbf{T}_1 \circ \mathbf{T}_2 = \mathbf{I}$, where $\mathbf{I}$ is the identity operator. Note that the above TD formulation is general and encompasses different alternatives such as time domain (when both $\mathbf{T}_1$ and $\mathbf{T}_2$ are identity operators) or frequency domain (when $\mathbf{T}_1$ is a Fast Fourier Transform (FFT) matrix and $\mathbf{T}_2$ is the Inverse Fast Fourier Transform (IFFT)) processing. RIM aims at reducing the impact of an interference $i[n]$ on the cleaned samples, $\bar{x}[n]$, which are used for the computation of the robust CAF [18]. Following the procedure shown

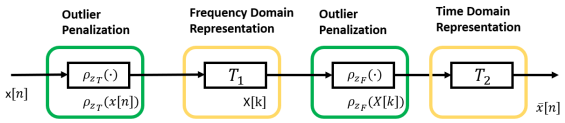

Fig. 3. DD-RIM with ZMNLs applied successively in the time and frequency domains. Green boxes indicate the application of a ZMNL and yellow boxes denote a linear transformation of the signal.

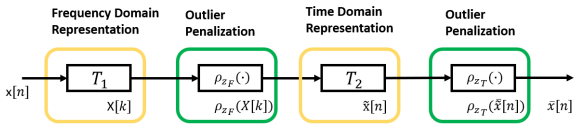

Fig. 4. DD-RIM with ZMNLs applied at first in the frequency and then in the time domain.

in Appendix A, a robust CAF after TD-RIM can be computed as:

$$\mathcal{C}_{\rho,i}(\boldsymbol{\kappa}) = \sum_{n=0}^{N-1} \bar{x}[n] c_i \left(nT_s - \tau_i(\boldsymbol{\kappa})\right) \mathrm{e}^{-j2\pi f_{d,i}(\boldsymbol{\kappa}) nT_s}, \tag{15}$$

which can be then used to solve for DPE's positioning solution in (11).

In essence, the robust CAF $\mathcal{C}_{\rho,i}(\boldsymbol{\kappa})$ applies a preprocessing to the data by means of a nonlinear function $\rho_z(x[n])$. A variety of nonlinearities can be employed to pre-process the signal that constructs the so-called robust CAF, as reviewed in Appendix B.

B. RIM in DD

Following the approach proposed in [23] for two-steps processing schemes, this section describes the implementation of ZMNLs in two consecutive domains, referred to as DD-RIM. It can be regarded as a cascade of two TD RIM processing blocks, for instance time and frequency domains. In particular, a doubly robust CAF is obtained as follows:

$$\mathcal{C}_{\rho,i}(\boldsymbol{\kappa}) = \sum_{n=0}^{N-1} \bar{x}[n] c_i \left(nT_s - \tau_i(\boldsymbol{\kappa})\right) \mathrm{e}^{-j2\pi f_{d,i}(\boldsymbol{\kappa}) nT_s}. \tag{16}$$

where $\bar{x}[n]$ are the time domain samples obtained after the sequential nonlinear processing on time and transformed domains as shown in Fig. 3, mathematically described as

$$\bar{x}[n] = \mathbf{T}_2 \left(\rho_{z_F}\left(X[k]\right)\right) \tag{17}$$

where

$$X[k] = \mathbf{T}_1 \left(\rho_{z_T}\left(x[n]\right)\right) \tag{18}$$

In this section, $\mathbf{T}_1$ and $\mathbf{T}_2$ are specified as FFT and IFFT, to bring the signal from the time to the frequency domains and vice versa. In general, other pairs of transformations could be used [17]. Estimates of the signal parameters are then obtained by maximizing the robust CAF as in (10).

As shown in Fig. 3, the received signal $x[n]$ is processed first with $\rho_{z_T}(\cdot)$ and then transformed into the frequency domain where $\rho_{z_F}(\cdot)$ is applied to get $\rho_{z_F}(X[k])$. Intuitively, the first nonlinearity would be in charge of mitigating outliers in the time domain (e.g. pulsed interferences) and the second nonlinearity of doing so in frequency (e.g. continuous wave interferences). The resulting cleaned signal, $\bar{x}[n] = \rho_{z_F}(X[k])$ can be used to compute the robust CAF (16) used for DD-RIM DPE processing as in (10). Conversely, Fig. 4 shows an alternative DD-RIM configuration, where the nonlinearities order is changed. In Fig, 4, DD-RIM approach is applied in the frequency domain first and then in the time domain. In detail, received signal $x[n]$ is transformed into the frequency domain signal, obtaining $X[k]$, which then is processed with RIM technique $\rho_{z_F}(\cdot)$ and transformed back into the time domain where a second ZMNL $\rho_{z_T}(\cdot)$ is applied.

IV. Loss of Efficiency

In robust statistics, an importance performance metric is the so-called *loss of efficiency*, or LoE for short. The LoE is the performance of the estimator under nominal conditions, which in the context of this work is in the absence of an interference. The rationale is to quantify the degradation of the robust method, compared to the optimal method when the nominal conditions hold. Ideally, one would like that LoE to be small. Previous works on RIM considered the output signal-to-noise-ratio (SNR) degradation in the absence of interferences for a number of ZMNLs [20]. Notice that in the DPE case, this approach is less intuitive since the robust methodology is used to compute a position solution jointly processing satellite signals. Therefore, in this article we derive the LoE for DPE-RIM in terms of its CRB degradation, which we will show it is indeed related to the SNR degradation of two-steps RIM. To achieve that result, the section first presents the CRB without RIM and then, secondly, the achievable CRB when RIM is considered. In particular we focus on Huber's nonlinearity due to its superior performance [20], [23]. transformations are considered. The LoE is then established as the difference between the former CRB and the RIM-based solutions.

A. Non-RIM

In order to obtain a more compact expression to compute the bound, we express (3) in vector form. Notice that, given that we are studying the LoE, the interference $i[n]$ is not accounted for. The resulting signal model is

$$\boldsymbol{x} = \boldsymbol{C}(\boldsymbol{\kappa})\boldsymbol{\alpha} + \boldsymbol{\eta}, \tag{19}$$

where $\boldsymbol{\alpha} = [\alpha_1, \alpha_2, \cdots, \alpha_M]^\top \in \mathbb{C}^{M\times 1}$ is the complex-value amplitude vector of each signal; the N signal samples are gathered in $\boldsymbol{x} = [x[0], \cdots, x[N-1]]^\top \in \mathbb{C}^{N\times 1}$ and $\boldsymbol{\eta} \in \mathbb{C}^{N\times 1}$ is a vector of N AWGN samples, each drawn from $\mathcal{CN}(0, \sigma_n^2)$. $\boldsymbol{C} = (\boldsymbol{c}_1, \boldsymbol{c}_2, \cdots, \boldsymbol{c}_M) \in \mathbb{C}^{N\times M}$ is the joint local replica, in which each column is generated for corresponding satellites and each row is generated

for different sampling instants. More concretely, we have

$$\boldsymbol{c}_i = \begin{bmatrix} s_i(-\tau_i(\boldsymbol{\kappa})) \\ s_i(T_s - \tau_i(\boldsymbol{\kappa}))\mathrm{e}^{(j2\pi f_{d,i}(\boldsymbol{\kappa})T_s)} \\ \vdots \\ s_i((N-1)T_s - \tau_i(\boldsymbol{\kappa}))\mathrm{e}^{(j2\pi f_{d,i}(\boldsymbol{\kappa})(N-1)T_s)} \end{bmatrix} = \begin{bmatrix} \omega_{i,0}(\boldsymbol{\kappa}) \\ \omega_{i,1}(\boldsymbol{\kappa}) \\ \vdots \\ \omega_{i,N-1}(\boldsymbol{\kappa}) \end{bmatrix} \tag{20}$$

Considering this vector form for the received signal model, the log-likelihood function is proportional to

$$\mathcal{L}(\boldsymbol{x}|\boldsymbol{\kappa}) = -\frac{1}{\sigma_n^2}\left[\boldsymbol{x} - \boldsymbol{C}(\boldsymbol{\kappa})\boldsymbol{\alpha}\right]^H \left[\boldsymbol{x} - \boldsymbol{C}(\boldsymbol{\kappa})\boldsymbol{\alpha}\right] . \tag{21}$$

Following the same derivation as in [32], the Fisher Information Matrix (FIM) is

$$\boldsymbol{\mathcal{I}}(\boldsymbol{\kappa}) = 2\boldsymbol{P}^\top \boldsymbol{\Xi}\boldsymbol{\Gamma}\boldsymbol{P}. \tag{22}$$

$\boldsymbol{\Gamma} = \mathrm{diag}(\boldsymbol{\gamma}^\top) = \mathrm{diag}([\mathrm{SNR}_1, \mathrm{SNR}_2, \cdots, \mathrm{SNR}_M]^\top) \in \mathbb{R}^{M\times M} = k_{\text{out}} \cdot \mathrm{diag}([\mathrm{SNR}_1^{\text{out}}, \mathrm{SNR}_2^{\text{out}}, \cdots, \mathrm{SNR}_M^{\text{out}}]^\top) \in \mathbb{R}^{M\times M}$ is the diagonal SNR matrix. $\boldsymbol{P}(\boldsymbol{\kappa}) = [\boldsymbol{P}_1^\top(\boldsymbol{\kappa}), \boldsymbol{P}_2^\top(\boldsymbol{\kappa}), \cdots, \boldsymbol{P}_M^\top(\boldsymbol{\kappa})]^\top \in \mathbb{R}^{M\times 3}$ is the concatenation of $\boldsymbol{P}_i(\boldsymbol{\kappa})$ from each satellite. The SNR_i denotes the prior-correlation SNR of the received signal from the i-th satellite

$$\mathrm{SNR}_i = \frac{1}{\sigma_n^2}\sum_{n=0}^{N-1} \omega_{i,n}^*(\boldsymbol{\kappa})\|\alpha_i\|^2\omega_{i,n}(\boldsymbol{\kappa}) = \frac{1}{\sigma_n^2}\sum_{n=0}^{N-1}\|\alpha_i\|^2 s_i^2(\boldsymbol{\kappa}), \tag{23}$$

and $\mathrm{SNR}_i^{\text{out}}$ denotes the corresponding post-correlation SNR while k_{out} is a scale parameter depending on the correlation form (i.e. correlation period, coherent correlation, noncoherent correlation). The mean quadratic bandwidth (MQBD) of the signal, ξ_i^2, is defined as

$$\xi_i^2 = \frac{\sum_{n=0}^{N-1} s_i'^2[n]}{\sum_{n=0}^{N-1} s_i^2[n]} = \frac{E_{s'}}{E_s} , \tag{24}$$

such that $\boldsymbol{\Xi} = \mathrm{diag}([\xi_1^2, \xi_2^2, \cdots, \xi_M^2]) \in \mathbb{R}^{M\times M}$ is the matrix form of MQBD. Typically, for a given GNSS constellation, a modulation scheme and a fixed bandwidth, the MQBD values are known and equal across signals of the same type. In other words, $\boldsymbol{\Xi} = \xi^2\mathbf{I} \in \mathbb{R}^{M\times M}$ if the M satellites are from the same constellation/signal. Recall that the inverse of the FIM in (22) provides the CRB for the parameters in $\boldsymbol{\kappa}$.

B. RIM in Time Domain

Comparing equation (10) and (11), we can identify that the difference between those two solutions (i.e. non-RIM and RIM) is the ZMNL $\rho_z(\cdot)$ applied to the received signal $x[n]$. Note that the same optimal solution for estimating $\boldsymbol{\theta}$ could be obtained when $x[n]$ is assumed as a heavy tailed distribution and when $\rho_z(x[n])$ is assumed to be Gaussian distributed. This section provides a CRB result under that assumption, which is then compared to the CRB in Section A to quantify the LoE.

In the previous section, we had a likelihood distribution of the form $\boldsymbol{x}|\boldsymbol{\kappa} \sim \mathcal{N}(\boldsymbol{C}(\boldsymbol{\kappa})\boldsymbol{\alpha}, \sigma_n^2\mathbf{I})$. Once the nonlinearity is applied to the data, the resulting likelihood is derived in Appendix C as $\rho_z(\boldsymbol{x})|\boldsymbol{\kappa} \sim \mathcal{N}(\boldsymbol{C}(\boldsymbol{\kappa})\bar{\boldsymbol{\alpha}}, \bar{\sigma}_n^2\mathbf{I})$, where $\bar{\boldsymbol{\alpha}}$ is the distorted signal amplitude after the pre-processing and $\bar{\sigma}_n^2$ is the modified noise variance, related to the original parameters by [20], [21]:

$$\bar{\boldsymbol{\alpha}} = \boldsymbol{\alpha}\left[1 - \mathrm{e}^{-\frac{T_h^2}{2\sigma_n^2}} + \frac{\sqrt{\pi}}{2}\frac{T_h}{\sqrt{2}\sigma_n}\mathrm{erfc}\left(\frac{T_h}{\sqrt{2}\sigma_n}\right)\right] \tag{25}$$

$$\bar{\sigma}_n^2 = \sigma_n^2\left[1 - \mathrm{e}^{-\frac{T_h^2}{2\sigma_n^2}}\right] . \tag{26}$$

when the ZMNL is Huber's (cf. Appendix B), with this relation changing depending on the class of nonlinearity.

Under the assumed Gaussian model after applying the ZMNL to the data, the corresponding FIM is:

$$\boldsymbol{\mathcal{I}}_\rho(\boldsymbol{\kappa}) = 2\boldsymbol{P}^\top\boldsymbol{\Xi}\bar{\boldsymbol{\Gamma}}\boldsymbol{P} , \tag{27}$$

where $\bar{\boldsymbol{\Gamma}} = \mathrm{diag}(\bar{\boldsymbol{\gamma}}) = \mathrm{diag}([\bar{\mathrm{SNR}}_1, \cdots, \bar{\mathrm{SNR}}_M]^\top) = k_{\text{out}} \cdot \mathrm{diag}([\bar{\mathrm{SNR}}_1^{\text{out}}, \cdots, \bar{\mathrm{SNR}}_M^{\text{out}}]^\top) \in \mathbb{R}^{M\times M}$ is composed of the SNRs of the satellites computed as in (23), but with the modified parameters in (25) and (26). Therefore, the CRB after Huber's nonlinearity is applied to $x[n]$, in the time domain, would be given by $\boldsymbol{\mathcal{I}}_\rho^{-1}(\boldsymbol{\kappa})$.

In order to define the LoE of the robust method, we consider the losses in (25) and (26) impact on the post-correlation SNR of each satellite as a reduction by $L(\sigma_n, T_h) = \frac{\bar{\mathrm{SNR}}_i^{\text{out}}}{\mathrm{SNR}_i^{\text{out}}}, i \in \{1, \ldots, M\}$. As a consequence, it is easy to see that $\boldsymbol{\mathcal{I}}^{-1}(\boldsymbol{\kappa}) = \boldsymbol{\mathcal{I}}_{\boldsymbol{\rho}}^{-1}(\boldsymbol{\kappa}) \cdot L(\sigma_n, T_h)$.

C. RIM in Transformed Domain

Following the processing chain in Fig. 2, we have $\bar{x}[n]$ as the output signal when the ZMNL function is applied in the transformed domain (in this case, the frequency domain which is the most common transformed domain in GNSS) [33]. Given the fact that $\mathbf{T}_1$ is a linear transformation, $X[k]$ is still Gaussian with expected value $\mathbb{E}\{X[k]\}$ and variance $\mathrm{Var}\{X[k]\}$. For instance, after the Huber's nonlinearity $\rho_z(\cdot)$, the mean and covariance of the resulting variable are modified as [20]:

$$\mathbb{E}\{\rho_z(X[k])\} = \mathbb{E}\{X[k]\}\left[1 - \mathrm{e}^{-\frac{T_h^2}{2\sigma_n^2}} + \frac{\sqrt{\pi}}{2}\frac{T_h}{\sqrt{2}\sigma_n}\mathrm{erfc}\left(\frac{T_h}{\sqrt{2}\sigma_n}\right)\right] \tag{28}$$

$$\mathrm{Var}\{\rho_z(X[k])\} = \mathrm{Var}\{X[k]\}\left[1 - \mathrm{e}^{-\frac{T_h^2}{2\sigma_n^2}}\right] . \tag{29}$$

When transforming the signal back to time domain, through the use of the linear transformation $\mathbf{T}_2$, several frequency samples $\rho_z(X[k])$ are combined to form the different time samples, $\bar{x}[n]$. By virtue of the Central Limit Theorem (CLT), [34] the resulting time domain signal $\bar{x}[n]$ can be considered to follow a Gaussian distribution as well [33]. Considering that $\mathbf{T}_2$ is also linear transform and $\mathbf{T}_1 \cdot \mathbf{T}_2 = \mathbf{I}$ is the identity operator (this holds for instance for FFT/IFFT operators), it was shown that $\bar{\boldsymbol{x}}|\boldsymbol{\kappa} \sim \mathcal{N}(\boldsymbol{C}(\boldsymbol{\kappa})\bar{\boldsymbol{\alpha}}, \bar{\sigma}_n^2\mathbf{I})$ has the same expected and

variance values as in (25) and (26). Following the same procedure as in earlier subsections, the FIM and CRB expressions can be obtained, respectively, as $\boldsymbol{I}_\rho(\boldsymbol{\kappa}) = 2\boldsymbol{P}^\top \boldsymbol{\Xi} \bar{\boldsymbol{\Gamma}} \boldsymbol{P}$ and $\mathbf{CRB}_\rho(\boldsymbol{\kappa}) = \boldsymbol{I}_\rho^{-1}(\boldsymbol{\kappa})$.

D. RIM in Dual Domain

Given the Gaussian assumption in RIM time domain processing and the CLT in RIM transformed domain processing, we can assume our processed signal $\bar{x}[n]$ as Gaussian distribution after RIM at DD following a similar derivation as in earlier subsections [23]. Therefore, the log-likelihood of processed signal after RIM DD processing is $\bar{\boldsymbol{x}}|\boldsymbol{\kappa} \sim \mathcal{N}(\boldsymbol{C}(\boldsymbol{\kappa})\bar{\boldsymbol{\alpha}}, \bar{\sigma}_n^2 \mathbf{I})$ where

$$\bar{\boldsymbol{\alpha}} = \boldsymbol{\alpha}\left[1 - \mathrm{e}^{-\frac{T_h^2}{2\sigma_n^2}} + \frac{\sqrt{\pi}}{2}\frac{T_h}{\sqrt{2}\sigma_n}\mathrm{erfc}\left(\frac{T_h}{\sqrt{2}\sigma_n}\right)\right]^2 \quad (30)$$

$$\bar{\sigma}_n^2 = \sigma_n^2\left[1 - \mathrm{e}^{-\frac{T_h^2}{2\sigma_n^2}}\right]^2. \quad (31)$$

Following the same procedure, we can derive the FIM and CRB as $\boldsymbol{I}_\rho(\boldsymbol{\kappa}) = 2\boldsymbol{P}^\top \boldsymbol{\Xi} \bar{\boldsymbol{\Gamma}} \boldsymbol{P}$ and $\mathbf{CRB}_\rho(\boldsymbol{\kappa}) = \boldsymbol{I}_\rho^{-1}(\boldsymbol{\kappa})$, respectively. $\bar{\mathrm{SNR}}_i$ represents the updated SNR of i-th satellite signal under influence of RIM method in frequency domain, and $\bar{\boldsymbol{\Gamma}}$, the corresponding SNR matrix.

V. Results

Different experiments were run in order to validate the propose RIM DPE methodology. In particular, we first assessed the theoretical LoE of the different RIM flavours by a simulation of I&Q samples from 7 GPS L1 C/A satellites. In this experiment, the SNR of each transmitted signal was set to be the same, with a sampling frequency of $f_s = 50$ MHz and a frontend low-pass filter of 2 MHz bandwidth. The receiver was simulated to be still at a fixed location. The LoE was computed by comparing the increase of Root Mean Square Error (RMSE) as a function of the carrier-to-noise-density ratio (CN0) when RIM approaches are applied in the standard case (that is, when RIM processing is not applied). Without loss of generality, in order to avoid numerical errors, we conducted the LoE experiments under a moderately high CN0 of 44 dB-Hz for DPE and 50 dB-Hz for 2SP method. In these simulations, the Accelerated Random Search (ARS) numerical optimization method was employed to optimize DPE cost function and estimate $\boldsymbol{\kappa}$ [30]. In the 2SP method, a Least Square (LS) method was used to estimate $\boldsymbol{\kappa}$ using the pseudoranges produced by a CAF maximization. The RMSE is computed after averaging $5 \cdot 10^4$ independent Monte Carlo experiments. Fig. 5 compares the LoE of various RIM approaches, both for DPE and 2SP methods, as a function of the normalized threshold T_h, an important parameter in Huber's non-linearity. In the figure, the black dashed lines represents the theoretical LoE of both single domain RIM (i.e. either time or frequency) and DD-RIM approaches, where

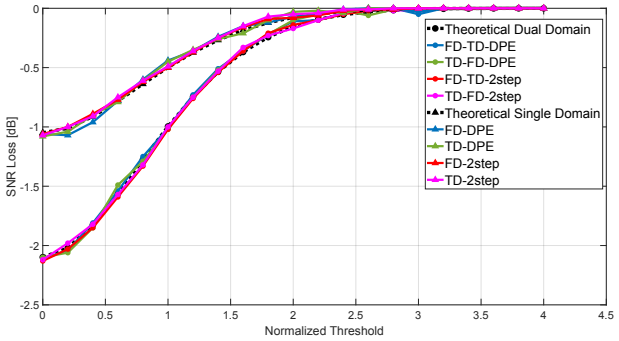

Fig. 5. LoE calculated from RMSE of position estimation under different RIM processing schemes.

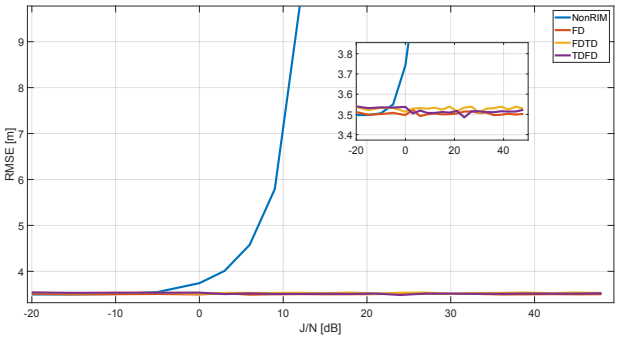

Fig. 6. RMSE of position estimation under different DPE RIM processing techniques in the presence of a CW jamming signal.

the line with circle represents DD-RIM approaches and the lines with triangles indicate single domain RIM. Similarly, the solid lines with circle also represent the experimentally computed LoE of DD-RIM approaches while those with triangles indicate experimental LoE of single domain RIM approaches. It can be observed that both DPE and 2SP approaches share the same LoE, given a RIM processing scheme. Overall, the results should good agreement between theoretical and experimental LoE, thus validating our LoE derivation.

Another set of experiments were performed in order to assess the robustness of RIM-DPE. In particular, simulations considering both CW and DME interferences were tested, which are discussed here. The strength of the interference was adjusted with the Jamming to Noise ratio (JN), defined as $\mathrm{JN} = \frac{\alpha_I^2}{\sigma_n^2}$ with α_I being the amplitude of the interference. Similarly as before, a simulation of I&Q samples from 7 GPS L5 C/A satellites was generated, with $\mathrm{CN0} = 44$ dB-Hz for all. The receiver employed a 20 MHz bandwidth low-pass filter and was static throughout the experiment, which consisted of 50 seconds worth of data. Note that the higher bandwidth is designed to include GPS L5. The threshold of Huber's ZMNL is chosen as $T_h = 1.345\hat{\sigma}_n$, which is generally picked to give reasonably high efficiency in the normal case, and the $\hat{\sigma}_n$ is calculated using the Median Absolute Deviation (MAR) of received signal: $\hat{\sigma}_n = \mathrm{MAR}/0.6745$ [35].

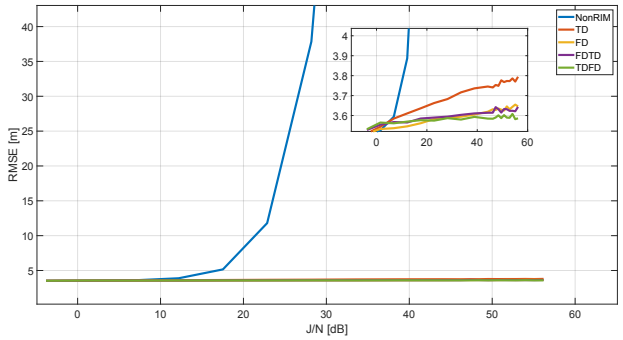

Fig. 7. RMSE of position estimation under different DPE RIM processing techniques in the presence of a DME interference signal.

Fig. 6 shows the various RIM approaches compared with the standard DPE non-RIM processing in the presence of a CW jamming signal, with JN varying from -20 dB to 48 dB. It can be observed that the case when RIM is not used, the presence of a CW jamming signal noticeably affects the estimation performance. In contrast, when DPE is used in conjunction with RIM processing techniques, the results show relatively stable performances over different CW power values. From the figure, we note that the best performance is achieved when a single non-linearity is applied directly in the frequency domain. This result is consistent to previous works considering two-steps processing [20], where it was noted that CWs are maximally concentrated in the frequency domain. Nevertheless, results show that the use of DD-RIM does not significantly degrade interference mitigation performance. Similarly, Fig. 7 shows the performance of the same set of DPE approaches, in this case under the presence of a DME interference signal, with JN varying from -4 dB to 56 dB. The received DME power was modeled in the simulations considering the Free-Space Path Loss Model (FSPLM). In general, RIM in one domain was not able to effectively mitigate DME signals and DD-RIM provides the best performance as compared with single-domain RIM techniques. The most effective approach was obtained when time-then-frequency domain processing was implemented. More specifically, time-then-frequency domain processing performed better than frequency-then-time domain processing. In the former, after time processing, the resulting signal is still relatively sparse in the frequency domain and thus it can be further mitigated using a robust non-linearity. In the second case, frequency processing does not produce an interfering signal that is sparse in time and that can be exploited by RIM in that domain. This ordering of RIM solutions is, again, consistent with the results for two-steps positioning reported in [20].

VI. Conclusions

Interference mitigation is crucial to protect GNSS from both intentional or unintentional interference signals. This paper presented the use of different RIM approaches within a direct-positioning framework. RIM has the desirable feature of avoiding the estimation of the interference signal, thus simplifying its implementation when compared to interference cancellation methods. Incorporating RIM augments the range of applicability of DPE in interference-rich situations, while DPE is already known to enhance the sensitivity of GNSS receivers to operate under weak signal conditions. The RIM methodology leverages results in robust statistics to design a new cross-ambiguity function and, consequently, a novel DPE cost function. In particular, this article explored the use of Huber's non-linearity for complex-valued signals, showing remarkable performance results under CW and DME interferences. Notice that RIM, which DPE-RIM is based on, is effective against interference signals that can be considered to be outliers in time and/or transformed domains, which encompass most of the known GNSS interference threats, although not all. This paper provided analytical expressions for the LoE of DPE RIM, that is, the degradation of performance caused by the proposed robust methods under nominal conditions when the interference signal is not present, showing negligible losses. DPE is a receiver framework that is known to provide enhanced sensitivity, enabling GNSS use in contested environments featuring weak signal conditions. The use of RIM in conjunction to DPE enables the high-sensitivity operation even under interference conditions. Future developments of DPE might involve its extension to high-accuracy applications.

Appendix A
Parameter estimation under RIM processing

This appendix provides the derivation of the estimator for $\boldsymbol{\kappa}$ and amplitudes $\alpha_1, \ldots, \alpha_M$ under RIM processing in a transformed domain, which results in the optimization of a robust version of the CAF. To achieve this goal, we take a twofold process. First, we linearize the general cost function using a first-order Taylor, as was done earlier in 2SP works. This is explained in equations (34) to (36). Secondly, to estimate the additional amplitude parameters $\alpha_1, \ldots, \alpha_M$, approximations based on the non-linearity are required, as derived in equations (45) and (48). Then, both results are combined in order to obtain a general robust CAF whose maximization would result in the RIM solution.

In RIM processing, the standard square error function is replaced by other choices that are able to attenuate the effect of model outliers. See Appendix B for an overview of those considered in the GNSS context of interest in this paper. Generally, the cost function to minimize under

M-estimation framework is:

$$J_\rho(\boldsymbol{\kappa}) = \sum_{k=0}^{N-1}(\rho(\mathbf{T}_1(x[k] - \sum_{i=1}^{M}\alpha_i c_i(kT_s - \tau_i(\boldsymbol{\kappa}))\mathrm{e}^{j(2\pi f_{d,i}(\boldsymbol{\kappa})nT_s+\phi_i)})))$$
$$= \sum_{n=0}^{N-1}\rho((\mathbf{T}_1(x[k]) - \mathbf{T}_1(\sum_{i=1}^{M}\alpha_i c_i(kT_s - \tau_i(\boldsymbol{\kappa}))\mathrm{e}^{j(2\pi f_{d,i}(\boldsymbol{\kappa})kT_s+\phi_i)})) \tag{32}$$

where $\rho(\cdot)$ is a cost function, which is a design choice that depends on the modeling assumptions. For instance, if $\rho(\cdot)$ is $|\cdot|^2$, we obtain the standard least squares solution, as shown in (10). $\mathbf{T}_1$ is the linear transforms defined in Section III-A. Note that $\mathbf{T}_1$ is a unitary matrix, satisfying $\mathbf{T}_1 \circ \mathbf{T}_1^H = \mathbf{I}$. In other words, $\mathbf{T}_2 = \mathbf{T}_1^H$. According to the fact that received GNSS signals are weak and the signal amplitude α_i can be assumed to be small compared to the noise term, $\rho(\cdot)$ can be expanded in Taylor series [18] for small amplitudes. Function $\rho(\cdot)$ can be regarded as a real function of two real variables, the real and imaginary parts of the complex signal. That is, with $z \in \mathbb{C}$ we can express:

$$\rho(z) = \rho(z_I, z_Q) \tag{33}$$

which, for a small increment $\Delta z = \Delta z_I + j\Delta z_Q$, can be expressed as

$$\begin{aligned}\rho(z - \Delta z) &= \rho(z_I - \Delta z_I, z_Q - \Delta z_Q)\\ &\backsimeq \rho(z) - \frac{\partial\rho(z)}{\partial z_I}\Delta z_I - \frac{\partial\rho(z)}{\partial z_Q}\Delta z_Q\\ &= \rho(z) - \Re\{\rho_z(z)\Delta z^*\}\end{aligned} \tag{34}$$

where z^* denotes complex conjugate of z and

$$\rho_z(z) = \rho_I(z) + j\rho_Q(z) = \frac{\partial\rho(z)}{\partial z_I} + j\frac{\partial\rho(z)}{\partial z_Q} = 2\frac{\partial\rho(z)}{\partial z^*} \tag{35}$$

$$\rho_{\bar{z}}(z) = \rho_I(z) - j\rho_Q(z) = \frac{\partial\rho(z)}{\partial z_I} - j\frac{\partial\rho(z)}{\partial z_Q} = 2\frac{\partial\rho(z)}{\partial z} \tag{36}$$

According to (34), (32) can be approximated as

$$J_\rho(\boldsymbol{\kappa}) \backsimeq \sum_{n=0}^{N-1}\rho(\mathbf{T}_1(x[k])) - \Re\{\sum_{k=0}^{N-1}\rho_z(\mathbf{T}_1(x[k]))\mathbf{T}_1(\sum_{i=1}^{M}\alpha_i c_i(kT_s - \tau_i(\boldsymbol{\kappa}))\mathrm{e}^{j(2\pi f_{d,i}(\boldsymbol{\kappa})kT_s+\phi_i)})^*\} \tag{37}$$

Since the first term in (37) does not depend on the parameter $\boldsymbol{\kappa}$, minimizing the cost function could be transformed into maximizing

$$\begin{aligned}J_{\text{real}}(\boldsymbol{\kappa}) &= \Re\{\sum_{k=0}^{N-1}\rho_z(\mathbf{T}_1(x[k]))\mathbf{T}_1(\sum_{i=1}^{M}\alpha_i c_i(kT_s - \tau_i(\boldsymbol{\kappa}))\mathrm{e}^{j(2\pi f_{d,i}(\boldsymbol{\kappa})kT_s+\phi_i)})^*\}\\ &\propto \Re\{\sum_{n=0}^{N-1}\mathbf{T}_2(\rho_z(\mathbf{T}_1(x[n])))\\ &\quad \mathbf{T}_2(\mathbf{T}_1(\sum_{i=1}^{M}\alpha_i c_i(nT_s - \tau_i(\boldsymbol{\kappa}))\mathrm{e}^{j(2\pi f_{d,i}(\boldsymbol{\kappa})nT_s+\phi_i)}))^*\}\\ &= \Re\{\sum_{n=0}^{N-1}\tilde{\rho}_z(x[n])\sum_{i=1}^{M}\alpha_i c_i(nT_s - \tau_i(\boldsymbol{\kappa}))\mathrm{e}^{-j(2\pi f_{d,i}(\boldsymbol{\kappa})nT_s+\phi_i)}\}\\ &= \Re\{\sum_{i=1}^{M}\sum_{n=0}^{N-1}\tilde{\rho}_z(x[n])\alpha_i c_i(nT_s - \tau_i(\boldsymbol{\kappa}))\mathrm{e}^{-j(2\pi f_{d,i}(\boldsymbol{\kappa})nT_s+\phi_i)}\}\\ &= \sum_{i=1}^{M}\alpha_i\Re\{\sum_{n=0}^{N-1}\tilde{\rho}_z(x[n])c_i(nT_s - \tau_i(\boldsymbol{\kappa}))\mathrm{e}^{-j(2\pi f_{d,i}(\boldsymbol{\kappa})nT_s+\phi_i)}\}\end{aligned} \tag{38}$$

which is a function of both $\boldsymbol{\kappa}$ and the amplitudes $\alpha_1, \ldots, \alpha_M$, and $\tilde{\rho}_z(x[n]) = \mathbf{T}_2(\rho_z(\mathbf{T}_1(x[n])))$.The proportional symbol in the equation above comes from the Parseval's theorem and the fact that $\mathbf{T}_1$ and $\mathbf{T}_2$ are linear and can be represented as unitary matrix. To achieve the optimal estimation of $\boldsymbol{\kappa}$, we first need to estimate the α_i:

$$\begin{aligned}\hat{\alpha}_i &= \arg\min_{\alpha_i}\sum_{k=0}^{N-1}\rho(\mathbf{T}_1(x[k] - \sum_{i=1}^{M}\alpha_i c_i(kT_s - \tau_i(\boldsymbol{\kappa}))\mathrm{e}^{j(2\pi f_{d,i}(\boldsymbol{\kappa})kT_s+\phi_i)}))\\ &= \arg\min_{\alpha_i}\sum_{k=0}^{N-1}\rho((\mathbf{T}_1(x[k]) - \mathbf{T}_1(\sum_{i=1}^{M}\alpha_i c_i(kT_s - \tau_i(\boldsymbol{\kappa}))\mathrm{e}^{j(2\pi f_{d,i}(\boldsymbol{\kappa})kT_s+\phi_i)}))\end{aligned} \tag{39}$$

whose derivative with respect to α_i is (following the chain rule):

$$\Re\{2\sum_{k=0}^{N-1}\mathbf{T}_1(c_i(kT_s - \tau_i(\boldsymbol{\kappa}))\mathrm{e}^{j(2\pi f_{d,i}(\boldsymbol{\kappa})kT_s+\phi_i)}) \rho_{\bar{z}}(\mathbf{T}_1(x[k] - \alpha_i c_i(kT_s - \tau_i(\boldsymbol{\kappa}))\mathrm{e}^{j(2\pi f_{d,i}(\boldsymbol{\kappa})kT_s+\phi_i)}))\} = 0 \tag{40}$$

The equation above can be further simplified when one accounts for the properties of the most common ZMNLs used in RIM processing, as reviewed in Appendix B. For instance, we can identify that the cost functions are all functions of the absolute value of a sample. Therefore we can further express (33) as:

$$\rho(z) = g(|z|) \tag{41}$$

with first derivative

$$\rho_z(z) = 2\frac{\partial g(|z|)}{\partial|z|}\frac{\partial|z|}{\partial z^*} = 2\frac{\partial g(|z|)}{\partial|z|}z \triangleq \frac{z}{h(|z|)} \tag{42}$$

where $h(|z|) \triangleq \frac{1}{2\frac{\partial g(|z|)}{\partial|z|}}$, and similarly we have:

$$\rho_{\bar{z}}(z) = 2\frac{\partial g(|z|)}{\partial|z|}\frac{\partial|z|}{\partial z} = 2\frac{\partial g(|z|)}{\partial|z|}z^* \triangleq \frac{z^*}{h(|z|)} \tag{43}$$

It can be seen that (41)is satisfied by the common ZMNL choices, cf. Appendix B, for instance observing that the different $\rho(\cdot)$ are a function of the magnitude of the argument. Using (43), we have:

$$\Re\{2\sum_{k=0}^{N-1}\mathbf{T}_1(c_i(kT_s - \tau_i(\boldsymbol{\kappa}))\mathrm{e}^{j(2\pi f_{d,i}(\boldsymbol{\kappa})kT_s+\phi_i)}) \frac{\mathbf{T}_1(x[k] - \alpha_i c_i(kT_s - \tau_i(\boldsymbol{\kappa}))\mathrm{e}^{j(2\pi f_{d,i}(\boldsymbol{\kappa})kT_s+\phi_i)})^*}{h(|\mathbf{T}_1(x[k] - \alpha_i c_i(kT_s - \tau_i(\boldsymbol{\kappa}))\mathrm{e}^{j(2\pi f_{d,i}(\boldsymbol{\kappa})kT_s+\phi_i)})|)}\} = 0 \tag{44}$$

Given that α_i is relatively small compared to $x[n]$, we have an approximation of the denominator term in as:

$$\Re\{2\sum_{n=0}^{N-1}\mathbf{T}_1(c_i(nT_s-\tau_i(\boldsymbol{\kappa}))\mathrm{e}^{j(2\pi f_{d,i}(\boldsymbol{\kappa})nT_s+\phi_i)}) \frac{\mathbf{T}_1(x[n]-\alpha_i c_i(nT_s-\tau_i(\boldsymbol{\kappa}))\mathrm{e}^{j(2\pi f_{d,i}(\boldsymbol{\kappa})nT_s+\phi_i)})^*}{h(|\mathbf{T}_1(x[n])|)}\}=0 \tag{45}$$

Considering the unitary property and linearity of the matrices corresponding to $\mathbf{T}_1$ and $\mathbf{T}_2$, as well as the Parseval's theorem, the equation above can be transformed as:

$$\Re\{2\sum_{n=0}^{N-1}\mathbf{T}_2(\mathbf{T}_1(c_i(nT_s-\tau_i(\boldsymbol{\kappa}))\mathrm{e}^{j(2\pi f_{d,i}(\boldsymbol{\kappa})nT_s+\phi_i)})) \mathbf{T}_2(\frac{\mathbf{T}_1(x[n]-\alpha_i c_i(nT_s-\tau_i(\boldsymbol{\kappa}))\mathrm{e}^{j(2\pi f_{d,i}(\boldsymbol{\kappa})nT_s+\phi_i)})}{h(|\mathbf{T}_1(x[n])|)})^*\}=0 \tag{46}$$

leading to

$$\begin{aligned}&\Re\{2\sum_{n=0}^{N-1}c_i(nT_s-\tau_i(\boldsymbol{\kappa}))\mathrm{e}^{j(2\pi f_{d,i}(\boldsymbol{\kappa})nT_s+\phi_i)}\mathbf{T}_2(\frac{\mathbf{T}_1(x[n])}{h(|\mathbf{T}_1(x[n])|)})^*\}\\&-\alpha_i\Re\{2\sum_{n=0}^{N-1}c_i(nT_s-\tau_i(\boldsymbol{\kappa}))\mathrm{e}^{j(2\pi f_{d,i}(\boldsymbol{\kappa})nT_s+\phi_i)}\\&\mathbf{T}_2(\frac{\mathbf{T}_1(c_i(nT_s-\tau_i(\boldsymbol{\kappa}))\mathrm{e}^{j(2\pi f_{d,i}(\boldsymbol{\kappa})nT_s+\phi_i)})}{h(|\mathbf{T}_1(x[n])|)})^*\}\\&=\Re\{2\sum_{n=0}^{N-1}c_i(nT_s-\tau_i(\boldsymbol{\kappa}))\mathrm{e}^{j(2\pi f_{d,i}(\boldsymbol{\kappa})nT_s+\phi_i)}\tilde{\rho}_z(x[n])^*\}\\&-\alpha_i\Re\{2\sum_{n=0}^{N-1}c_i(nT_s-\tau_i(\boldsymbol{\kappa}))\mathrm{e}^{j(2\pi f_{d,i}(\boldsymbol{\kappa})nT_s+\phi_i)}\\&\mathbf{T}_2(\frac{\mathbf{T}_1(c_i(nT_s-\tau_i(\boldsymbol{\kappa}))\mathrm{e}^{j(2\pi f_{d,i}(\boldsymbol{\kappa})nT_s+\phi_i)})}{h(|\mathbf{T}_1(x[n])|)})^*\}=0\end{aligned} \tag{47}$$

Given that RIM processing is based on the assumption that the interference component occurs as sparse representation in the processed domain and few samples are affected, we have the assumption that $h(|\mathbf{T}_1(\boldsymbol{x})|)\propto\mathbf{I}$, where $\boldsymbol{x}$ is a vector with $x[n]$ as its n-th element. With this assumption, we have

$$\Re\{2\sum_{n=0}^{N-1}c_i(nT_s-\tau_i(\boldsymbol{\kappa}))\mathrm{e}^{j(2\pi f_{d,i}(\boldsymbol{\kappa})nT_s+\phi_i)} \mathbf{T}_2(\frac{\mathbf{T}_1(c_i(nT_s-\tau_i(\boldsymbol{\kappa}))\mathrm{e}^{j(2\pi f_{d,i}(\boldsymbol{\kappa})nT_s+\phi_i)})}{h(|\mathbf{T}_1(x[n])|)})^*\}\propto 2N \tag{48}$$

leading to

$$\begin{aligned}\hat{\alpha}_i&\propto\Re\{\sum_{n=0}^{N-1}c_i(nT_s-\tau_i(\boldsymbol{\kappa}))\mathrm{e}^{j(2\pi f_{d,i}(\boldsymbol{\kappa})nT_s+\phi_i)}\tilde{\rho}_z(x[n])^*\}\\&=\Re\{\sum_{n=0}^{N-1}c_i(nT_s-\tau_i(\boldsymbol{\kappa}))\mathrm{e}^{-j(2\pi f_{d,i}(\boldsymbol{\kappa})nT_s+\phi_i)}\tilde{\rho}_z(x[n])\}\end{aligned} \tag{49}$$

Substituting (49) into (38), we have $J_{\text{real}}(\boldsymbol{\kappa})$ as

$$\begin{aligned}J_{\text{real}}(\boldsymbol{\kappa})&\propto\sum_{i=1}^{M}\Re\{\sum_{n=0}^{N-1}\tilde{\rho}_z(x[n])c_i(nT_s-\tau_i(\boldsymbol{\kappa}))\mathrm{e}^{-j(2\pi f_{d,i}(\boldsymbol{\kappa})nT_s+\phi_i)}\}^2\\&=\sum_{i=1}^{M}\Re\{\mathcal{C}_{\rho,i}(\boldsymbol{\kappa})\mathrm{e}^{-j\phi_i}\}^2\\&=\sum_{i=1}^{M}\Re\{\left|\mathcal{C}_{\rho,i}(\boldsymbol{\kappa})\right|\mathrm{e}^{j(\angle\mathcal{C}_{\rho,i}(\boldsymbol{\kappa})-\phi_i)}\}^2\\&=\sum_{i=1}^{M}\left(\left|\mathcal{C}_{\rho,i}(\boldsymbol{\kappa})\right|\Re\{\mathrm{e}^{j(\angle\mathcal{C}_{\rho,i}(\boldsymbol{\kappa})-\phi_i)}\}\right)^2\\&=\sum_{i=1}^{M}\left(\left|\mathcal{C}_{\rho,i}(\boldsymbol{\kappa})\right|\cos(\angle\mathcal{C}_{\rho,i}(\boldsymbol{\kappa})-\phi_i)\right)^2\end{aligned} \tag{50}$$

According to (50), the cost function is factored in two terms. The first is the absolute value of the CAF and depends only on κ. The second term is a cosine which also depends on ϕ_i. The cosine can be maximised by setting with $\hat{\phi}_i=\angle\mathcal{C}_{\rho,i}(\boldsymbol{\kappa})$, we can further convert the optimization of (50) to:

$$\hat{\boldsymbol{\kappa}}=\arg\max_{\boldsymbol{\kappa}}\sum_{i=1}^{M}|\mathcal{C}_{\rho,i}(\boldsymbol{\kappa})|^2 \tag{51}$$

where $\mathcal{C}_{\rho,i}(\boldsymbol{\kappa})$ is the robust version of CAF define as

$$\mathcal{C}_{\rho,i}(\boldsymbol{\kappa})=\tilde{\rho}_z(x[n])c_i(nT_s-\tau_i(\boldsymbol{\kappa}))\mathrm{e}^{-j2\pi f_{d,i}(\boldsymbol{\kappa})nT_s}\ . \tag{52}$$

Appendix B
Selected Non-linearities for RIM processing

This appendix provides an overview of some RIM non-linearities considered in the GNSS context of interest. In GNSS signal processing, the most common cost functions $\rho(z)$ are introduced in [17], [36], [37], among which three of the ZMNLs as well as the corresponding cost functions are listed in this section as examples:

1) Laplacian model assumption for the likelihood distribution [19]. The cost function $\rho(z)$ is:

$$\rho(z)=|z| \tag{53}$$

Then, the ZMNL function $\rho_z(z)$ in (14) can be obtained as (36):

$$\rho_z(z)=\frac{z}{|z|}\triangleq\rho_z(z)\qquad\text{for } z\neq 0 \tag{54}$$

The ZMNL in (54) is referred to as *complex signum* ZMNL according to [38]. Furthermore, we have that

$$\rho_{zz}(z)=\frac{-z^2}{|z|^3}\qquad\text{for } z\neq 0\ , \tag{55}$$

as needed with the DPE RIM framework discussed in this paper.

2) Cauchy model assumption for the likelihood distribution [18]. The cost function $\rho(z)$ is:

$$\rho(z)=\frac{3}{2}\log(K_C+|z|^2)+\frac{1}{2}\log(\frac{4\pi^2}{K_C}) \tag{56}$$

where K_C is referred to as the linearity parameter [39]. The corresponding *myriad* ZMNL is:

$$\rho_z(z)=\frac{K_C z}{K_C+|z|^2} \tag{57}$$

with

$$\rho_{zz}(z) = \frac{-K_C z^2}{(K_C + |z|^2)^2} \tag{58}$$

3) M-estimation based on Huber's loss [20] The cost function $\rho(z)$ is defined as:

$$\rho(z) = \begin{cases} \frac{1}{2}|z|^2 & \text{for } |z| \leq T_h \\ T_h|z| - \frac{1}{2}T_h^2 & \text{for } |z| > T_h \end{cases} \tag{59}$$

By using (36), the resulting ZMNL $\rho_z(z)$ is:

$$\rho_z(z) \triangleq \rho_z(z) = \begin{cases} z & \text{for } |z| \leq T_h \\ T_h \text{ csign}(z) & \text{for } |z| > T_h \end{cases} \tag{60}$$

where T_h is a decision threshold, that is a tuning constant [37], and csign(z) is defined as:

$$\text{csign}(z) = \begin{cases} \frac{z}{|z|} & \text{for } z \neq 0 \\ 0 & \text{for } z = 0 \end{cases} . \tag{61}$$

such that

$$\rho_{zz}(z) = \begin{cases} 0 & \text{otherwise} \\ T_h \frac{-z^2}{|z|^3} & \text{for} |z| > T_h \text{ and } z \neq 0 \end{cases} \tag{62}$$

Appendix C
Maximum likelihood estimation after RIM non-linearity

This appendix shows the derivation of maximum likelihood estimator of $\boldsymbol{\kappa}$ once the RIM nonlinearity is applied. The Gaussian model assumption is shown in subsection IV. B. To estimate $\boldsymbol{\kappa}$, the maximum likelihood estimator is applied in (63):

$$\begin{aligned} \hat{\boldsymbol{\kappa}} &= \arg\min_{\boldsymbol{\kappa}} J_\rho(\boldsymbol{\kappa}) \\ &= \arg\min_{\boldsymbol{\kappa}} \left[\rho_z(\boldsymbol{x}) - \boldsymbol{C}(\boldsymbol{\kappa})\bar{\boldsymbol{\alpha}}\right]^H \left[\rho_z(\boldsymbol{x}) - \boldsymbol{C}(\boldsymbol{\kappa})\bar{\boldsymbol{\alpha}}\right] \end{aligned} \tag{63}$$

where $\bar{\boldsymbol{\alpha}}$ is the distorted signal amplitude after the non-linearity processing, related to the original parameters by [20], [21]. To minimize the cost function, we first take derivative w.r.t. $\bar{\boldsymbol{\alpha}}$ and setting it to zero yields to

$$\hat{\bar{\boldsymbol{\alpha}}} = (\boldsymbol{C}^H\boldsymbol{C})^{-1}\boldsymbol{C}^H\rho_z(\boldsymbol{x}). \tag{64}$$

which turns in to $\hat{\bar{\boldsymbol{\alpha}}} = \boldsymbol{C}^H\rho_z(\boldsymbol{x})$, given the property that $\boldsymbol{C}^H\boldsymbol{C} \approx \boldsymbol{I}$ [12]. Substituting equation (64) into equation (63), it can be seen that

$$\begin{aligned} J_\rho(\boldsymbol{\kappa}) &= \left[\rho_z(\boldsymbol{x}) - \boldsymbol{C}(\boldsymbol{\zeta})\hat{\bar{\boldsymbol{\alpha}}}\right]^H \left[\rho_z(\boldsymbol{x}) - \boldsymbol{C}(\boldsymbol{\zeta})\hat{\bar{\boldsymbol{\alpha}}}\right] \\ &= \|\boldsymbol{C}^H\rho_z(\boldsymbol{x})\|^2 = \mathcal{C}_{\rho,i}(\boldsymbol{\kappa}) \, . \end{aligned} \tag{65}$$

which is the vector form of the robust CAF in (15). This equality shows that the Gaussian assumption on $\rho_z(x[n])$ leads to the same $\boldsymbol{\kappa}$ estimation as under the actual distribution, as shown in Appendix A. As a consequence, this modeling assumption can be used to derive the estimation bounds, which greatly simplifies the calculations.

REFERENCES

[1] E. D. Kaplan and C. Hegarty, *Understanding GPS/GNSS: Principles and applications*. Artech house, 2017.

[2] K. Borre and D. Akos, "A software-defined gps and galileo receiver: single-frequency approach," in *Proceedings of the 18th International Technical Meeting of the Satellite Division of The Institute of Navigation (ION GNSS 2005)*, 2005, pp. 1632–1637.

[3] Y. J. Morton, F. van Diggelen, J. J. Spilker Jr, B. W. Parkinson, S. Lo, and G. Gao, *Position, navigation, and timing technologies in the 21st century: Integrated satellite navigation, sensor systems, and civil applications, volume 1*. John Wiley & Sons, 2021.

[4] R. A. Iltis and L. Mailaender, "An adaptive multiuser detector with joint amplitude and delay estimation," *IEEE Journal on Selected Areas in Communications*, vol. 12, no. 5, pp. 774–785, 1994.

[5] A. Amar and A. J. Weiss, "New asymptotic results on two fundamental approaches to mobile terminal location," in *2008 3rd International Symposium on Communications, Control and Signal Processing*. IEEE, 2008, pp. 1320–1323.

[6] P. Closas and G. Gao, "Direct Position Estimation," 2021.

[7] P. Closas, C. Fernández-Prades, and J. A. Fernández-Rubio, "Maximum likelihood estimation of position in gnss," *IEEE Signal Processing Letters*, vol. 14, no. 5, pp. 359–362, 2007.

[8] T. Pany, *Navigation signal processing for GNSS software receivers*. Artech House, 2010.

[9] A. Steingass and A. Lehner, "Measuring the navigation multipath channel: a statistical analysis," in *Proceedings of the 17th International Technical Meeting of the Satellite Division of The Institute of Navigation (ION GNSS 2004)*, 2004, pp. 1157–1164.

[10] P. Closas, C. Fernández-Prades, A. Fernández, M. Wis, G. Vecchione, F. Zanier, J. Garcia-Molina, and M. Crisci, "Evaluation of GNSS direct position estimation in realistic multipath channels," in *Proceedings of the 28th International Technical Meeting of the Satellite Division of The Institute of Navigation (ION GNSS+ 2015)*, 2015, pp. 3693–3701.

[11] M. G. Amin, P. Closas, A. Broumandan, and J. L. Volakis, "Vulnerabilities, threats, and authentication in satellite-based navigation systems [scanning the issue]," *Proceedings of the IEEE*, vol. 104, no. 6, pp. 1169–1173, 2016.

[12] G. X. Gao, "DME/TACAN Interference and its Mitigation in L5/E5 Bands," in *ION Institute of Navigation Global Navigation Satellite Systems Conference*, 2007.

[13] R. T. Ioannides, T. Pany, and G. Gibbons, "Known vulnerabilities of global navigation satellite systems, status, and potential mitigation techniques," *Proceedings of the IEEE*, vol. 104, no. 6, pp. 1174–1194, 2016.

[14] J. Arribas, J. Vilà-Valls, A. Ramos, C. Fernández-Prades, and P. Closas, "Air traffic control radar interference event in the Galileo E6 band: Detection and localization," *Navigation*, vol. 66, no. 3, pp. 505–522, 2019.

[15] D. Borio and E. Cano, "Optimal global navigation satellite system pulse blanking in the presence of signal quantisation," *IET Signal Processing*, vol. 7, no. 5, pp. 400–410, 2013.

[16] D. Borio, L. Camoriano, and L. L. Presti, "Two-pole and multi-pole notch filters: a computationally effective solution for GNSS interference detection and mitigation," *IEEE Systems Journal*, vol. 2, no. 1, pp. 38–47, 2008.

[17] D. Borio and P. Closas, "A fresh look at GNSS anti-jamming," *Inside GNSS*, no. 5, 2017.

[18] D. Borio, "Myriad non-linearity for GNSS robust signal processing," *IET Radar, Sonar & Navigation*, vol. 11, no. 10, pp. 1467–1476, 2017.

[19] B. Daniele and C. Pau, "Complex signum non-linearity for robust GNSS interference mitigation," *IET Radar, Sonar & Navigation*, vol. 12, no. 8, pp. 900–909, 2018.

[20] D. Borio, H. Li, and P. Closas, "Huber's non-linearity for GNSS interference mitigation," *Sensors*, vol. 18, no. 7, p. 2217, 2018.

[21] ——, "Huber's Non-linearity for Robust Transformed Domain GNSS Signal Processing," in *Proceedings of the 31st Inter-*

national Technical Meeting of the Satellite Division of The Institute of Navigation (ION GNSS+ 2018), 2018, pp. 3775–3787.

[22] H. Li, "Robust interference mitigation methods for GNSS anti-jamming," Master's thesis, Northeastern University, 2018.

[23] H. Li, D. Borio, and P. Closas, "Dual-domain robust GNSS interference mitigation," in *Proceedings of the 32nd International Technical Meeting of the Satellite Division of The Institute of Navigation (ION GNSS+ 2019)*, 2019, pp. 991–1002.

[24] C. Gioia and D. Borio, "Multi-layered Multi-constellation GNSS Interference Mitigation," in *Proceedings of the 34th International Technical Meeting of the Satellite Division of The Institute of Navigation (ION GNSS+ 2021)*, 2021, pp. 1796–1808.

[25] C. Fernández-Prades, J. Arribas, and P. Closas, "Robust GNSS receivers by array signal processing: Theory and implementation," *Proceedings of the IEEE*, vol. 104, no. 6, pp. 1207–1220, 2016.

[26] P. Closas and A. Gusi-Amigo, "Direct position estimation of GNSS receivers: Analyzing main results, architectures, enhancements, and challenges," *IEEE Signal Processing Magazine*, vol. 34, no. 5, pp. 72–84, 2017.

[27] D. Borio, F. Dovis, H. Kuusniemi, and L. L. Presti, "Impact and detection of GNSS jammers on consumer grade satellite navigation receivers," *Proceedings of the IEEE*, vol. 104, no. 6, pp. 1233–1245, 2016.

[28] R. Morales-Ferre, P. Richter, E. Falletti, A. de la Fuente, and E. S. Lohan, "A survey on coping with intentional interference in satellite navigation for manned and unmanned aircraft," *IEEE Communications Surveys & Tutorials*, vol. 22, no. 1, pp. 249–291, 2019.

[29] U. Epple, F. Hoffmann, and M. Schnell, "Modeling DME interference impact on LDACS1," in *2012 Integrated Communications, Navigation and Surveillance Conference*. IEEE, 2012, pp. G7–1.

[30] P. Closas, "Bayesian signal processing techniques for GNSS receivers: from multipath mitigation to positioning," Ph.D. dissertation, Universitat Politècnica de Catalunya, 2009.

[31] S. Tang, H. Li, H. Calatrava, and P. Closas, "Precise Direct Position Estimation: Validation Experiments," in *Proc. of the IEEE/ION PLANS*, Monterey, CA, April 2023.

[32] A. G. Amigó, P. Closas, A. Mallat, and L. Vandendorpe, "Cramér-Rao bound analysis of UWB based localization approaches," in *2014 IEEE International Conference on Ultra-WideBand (ICUWB)*. IEEE, 2014, pp. 13–18.

[33] D. Borio and P. Closas, "Robust transform domain signal processing for GNSS," *Navigation*, vol. 66, no. 2, pp. 305–323, 2019.

[34] G. Casella and R. L. Berger, *Statistical inference*. Cengage Learning, 2021.

[35] J. Fox and S. Weisberg, "Robust regression," *An R and S-Plus companion to applied regression*, vol. 91, p. 6, 2002.

[36] P. J. Huber, "Robust estimation of a location parameter," *The annals of mathematical statistics*, pp. 73–101, 1964.

[37] ——, "Robust statistics," in *International encyclopedia of statistical science*. Springer, 2011, pp. 1248–1251.

[38] D. Borio and P. Closas, "Complex signum non-linearity for robust GNSS signal processing," *IET Radar Sonar and Navigation*, pp. 1–9, April 2018.

[39] G. R. Arce, *Nonlinear signal processing: a statistical approach*. John Wiley & Sons, 2005.

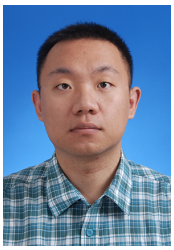

Haoqing Li received the B.S. degree in electrical engineering from Wuhan University, China, in 2016 and the M.S. degree in electrical and computer engineering from Northeastern University, Boston, MA, in 2018, where he is currently working toward the Ph.D. degree in electrical and computer engineering. His research interests include GNSS signal processing, anti-jamming technology, and robust statistics.

Shuo Tang received the B.S. degree in mechanical engineering from China Agricultural University, China and the M.S. degree in mechanical engineering from Northeastern University, Boston, MA, in 2014 and 2018, respectively. He is currently working as a Ph.D. candidate in electrical and computer engineering at Northeastern University. His research interests include GNSS signal processing, sensor fusion and computational statistics.

Peng Wu received his B.S. degree in Physics from Tianjin University of Technology, China and M.S. degree in Electrical Engineering from Northeastern University, Boston, MA. He is currently a Ph.D. candidate in the Department of Electrical and Computer Engineering at Northeastern University. His research interests include distributed data fusion and machine learning with applications to indoor positioning and tracking.

Pau Closas (Senior Member, IEEE), is an Associate Professor in Electrical and Computer Engineering at Northeastern University, Boston MA. He received the M.S. and Ph.D. in Electrical Engineering from UPC in 2003 and 2009, respectively. He also holds a M.S. in Advanced Maths and Mathematical Engineering from UPC since 2014. He is the recipient of the EURASIP Best PhD Thesis Award 2014, the 9^{th} Duran Farell Award for Technology Research, the 2016 ION's Early Achievements Award, 2019 NSF CAREER Award, and the IEEE AESS Harry Rowe Mimno Award in 2022. His primary areas of interest include statistical signal processing, stochastic filtering, robust filtering, and machine learning, with applications to positioning and localization systems. He volunteered in editorial roles (e.g. NAVIGATION, Proc. IEEE, IEEE Trans. Veh. Tech., and IEEE Sig. Process. Mag.), and has been actively involved in organizing committees of a number of conference such as EUSIPCO (2011, 2019-2022), IEEE SSP'16, IEEE/ION PLANS (2020, 2023), or IEEE ICASSP'20.